Electronic Supplementary Material (ESI) for New Journal of Chemistry.

Supporting Information

Tuning oxygen vacancies in MoS_2@MoO_2 hierarchical tubular heterostructure for high performance lithium-ion batteries

Chaofei Guo, Yaomeng Yao, YingNan Cao, Qin Feng, Yifan Zhang and Yong Wang**

Department of Chemical Engineering, School of Environmental and Chemical Engineering, Shanghai University, 99 Shangda Road, Shanghai 200444, P. R. China.

*Corresponding authors: Tel: +86-21-66137723; fax: +86-21-66137725.

Email address: yongwang@shu.edu.cn；zyf010626@shu.edu.cn

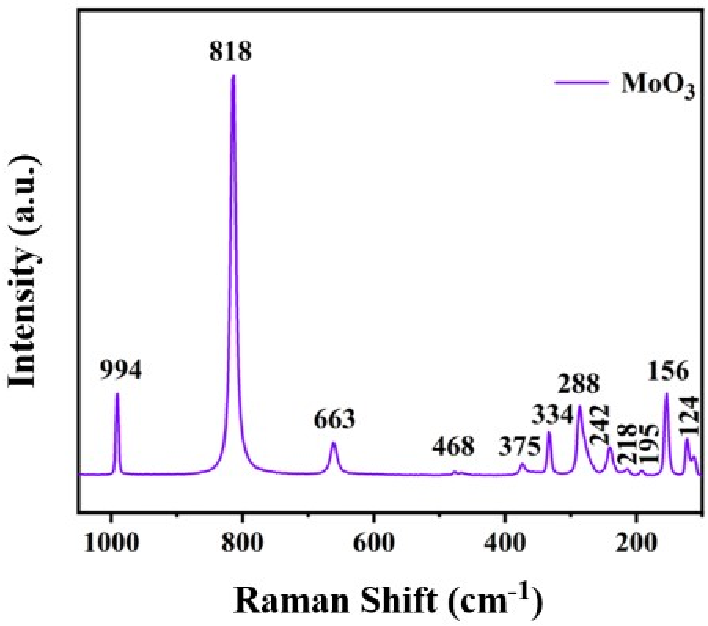

Fig. S1. The Raman spectrum of MoO_3, the peaks at 994, 818, 663, 468, 375, 334, 288, 242, 218, 195, 156 and 124 cm^{-1} corresponding to its typical characteristics peaks. The peaks at 996 cm^{-1} indicates the stretching vibration of terminal Mo=O (Ag mode) along a- and b-axes, the peak at 819 cm^{-1} indicates the doubly coordinated oxygen (Mo-O-Mo) stretching mode, and the triply coordinated oxygen (Mo-O) stretching mode located at 667 cm^{-1}).

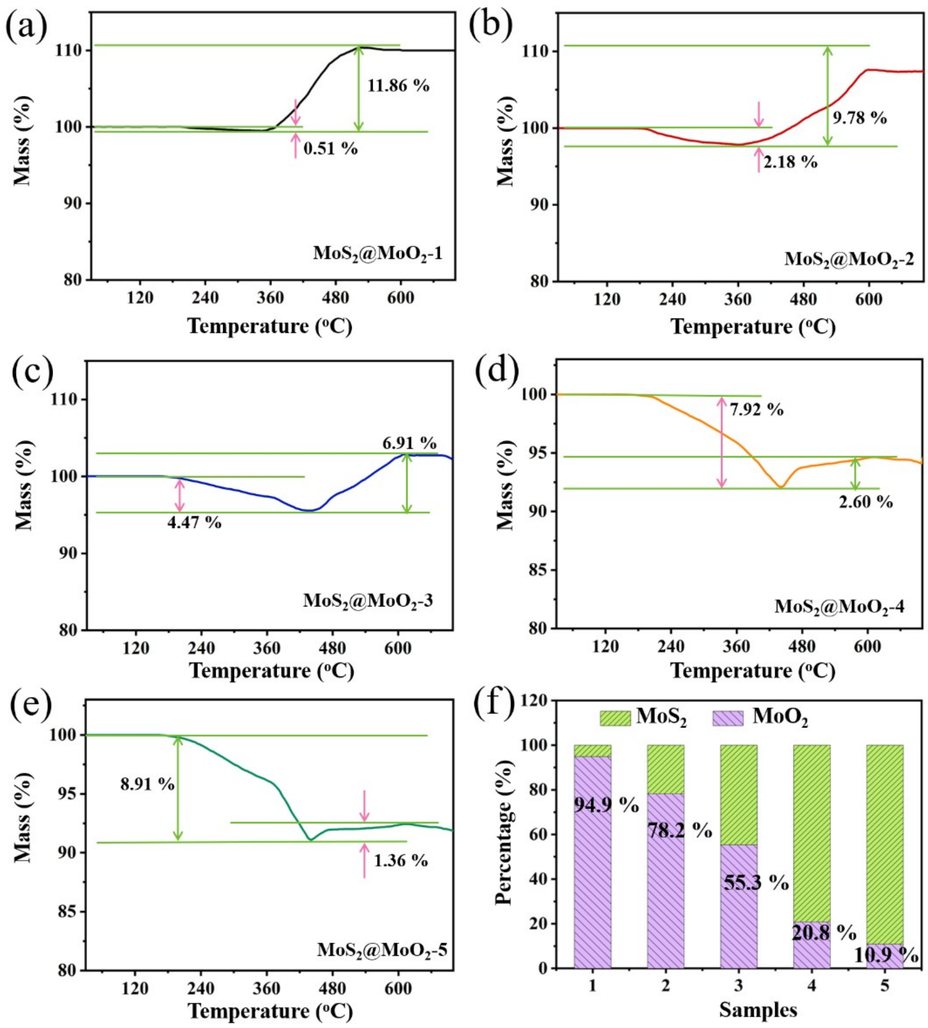

Fig. S2 TG curves of (a) MoS_2@MoO_2-1, (b) MoS_2@MoO_2-2, (c) MoS_2@MoO_2-3, (d) MoS_2@MoO_2-4 and (e) MoS_2@MoO_2-5. (f) The weight contents of MoO_2 and MoS_2 in MoS_2@MoO_2-1, MoS_2@MoO_2-2, MoS_2@MoO_2-3, MoS_2@MoO_2-4, and MoS_2@MoO_2-5 composite.

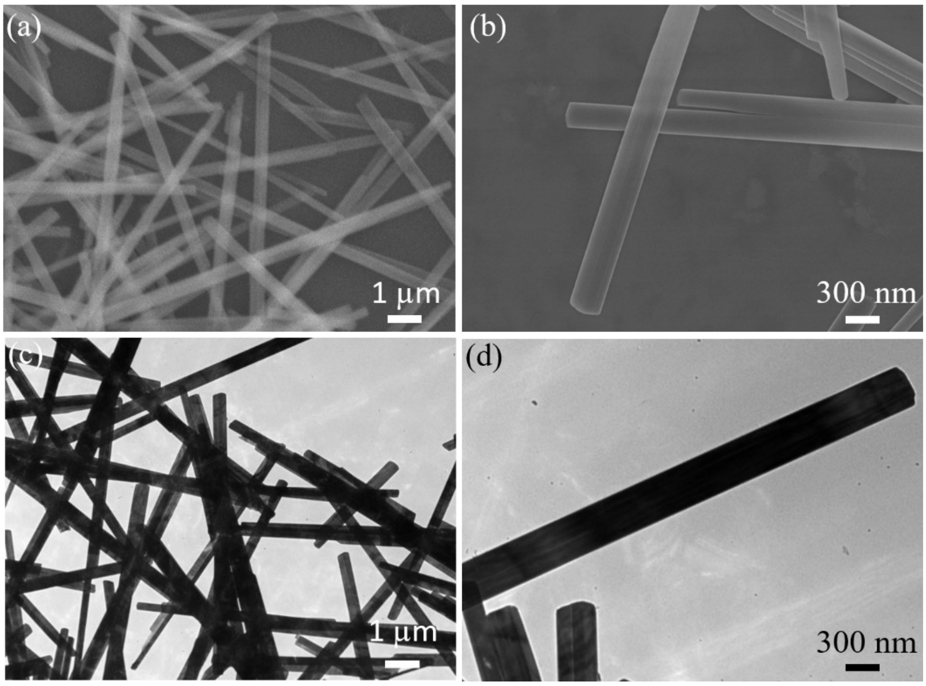

Fig. S3. (a-b) SEM images of MoO_3; (c-d) TEM images of MoO_3.

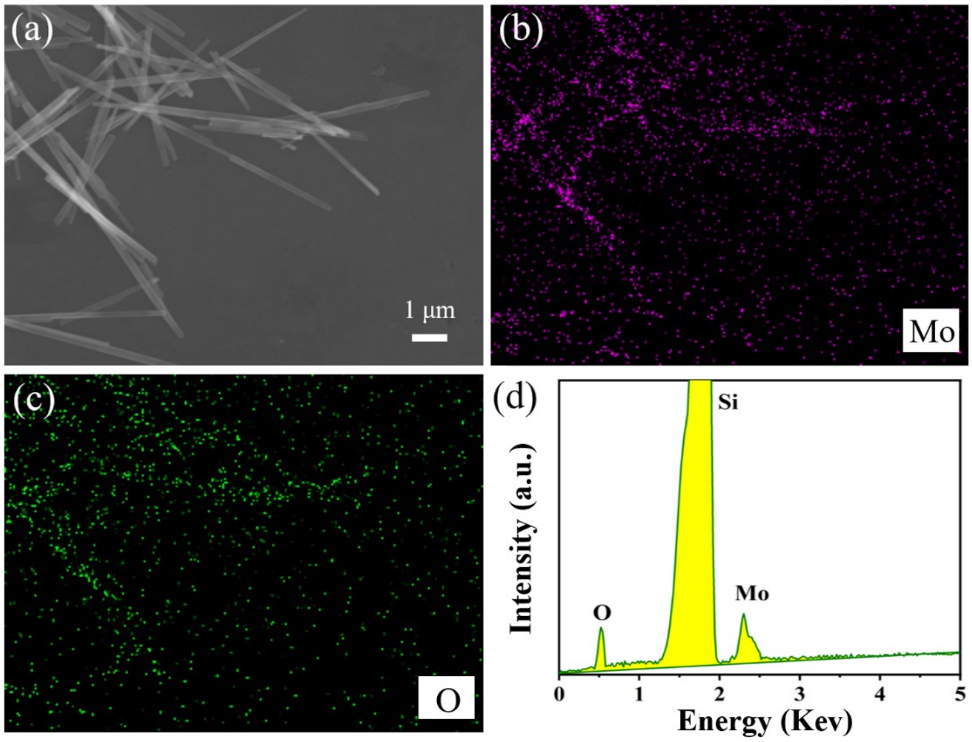

Fig. S4. (a) SEM image of MoO_3 and (b-c) the corresponding EDS mapping of Mo and O; (d) EDS spectra of MoO_3.

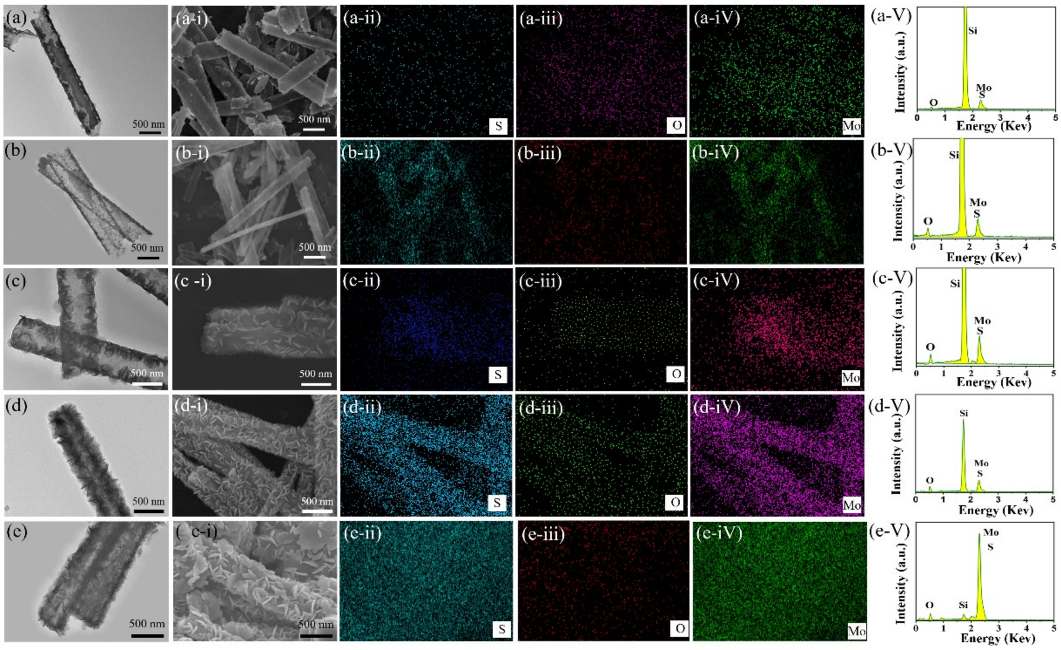

Fig. S5. (a) and a-i) TEM and SEM images of MoS_2@MoO_2-1, (a-i)-(a-iV) the elemental mapping images of MoS_2@MoO_2-1, (a-v) EDS spectra; (b) and (b-i) TEM and SEM images of MoS_2@MoO_2-2, (b-i)-(b-iv) the elemental mapping images of MoS_2@MoO_2-2, (a-v) EDS spectra; (c) and (c-i) TEM and SEM images of MoS_2@MoO_2-3, (c-i)-(c-iV) the elemental mapping images of MoS_2@MoO_2-3, (c-v) EDS spectra; (d) and (d-i) TEM and SEM images of MoS_2@MoO_2-1, (d-i)-(d-iV) the elemental mapping images of MoS_2@MoO_2-1, (d-v) EDS spectra; (e) and (e-i) the TEM and SEM images of MoS_2@MoO_2-1, (e-i)-(e-iV) the elemental mapping images of MoS_2@MoO_2-1, (e-v) EDS spectra.

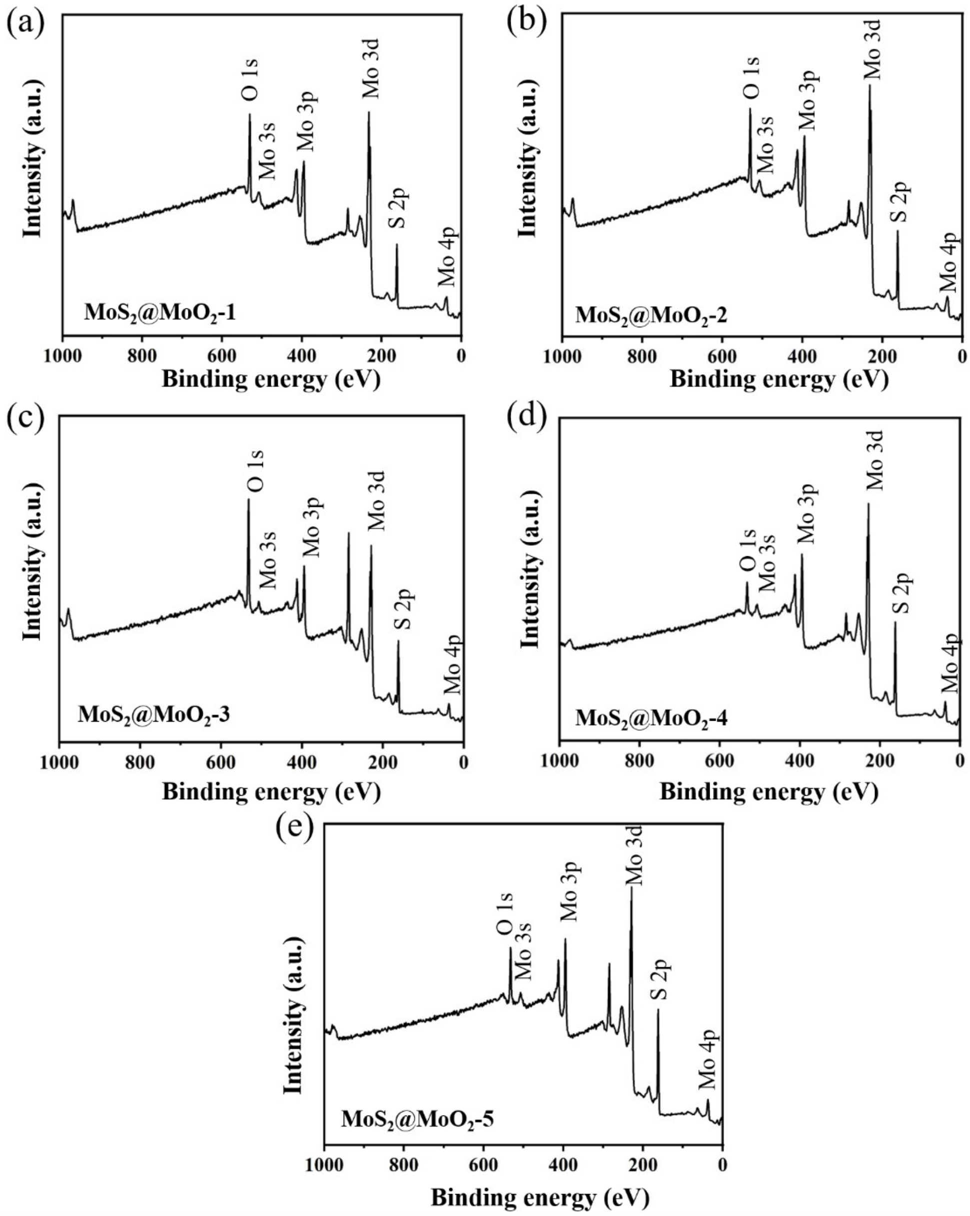

Fig. S6. (a-e) The XPS survey spectrum of MoS_2@MoO_2-1, MoS_2@MoO_2-2, MoS_2@MoO_2-3, MoS_2@MoO_2-4 and MoS_2@MoO_2-5, respectively.

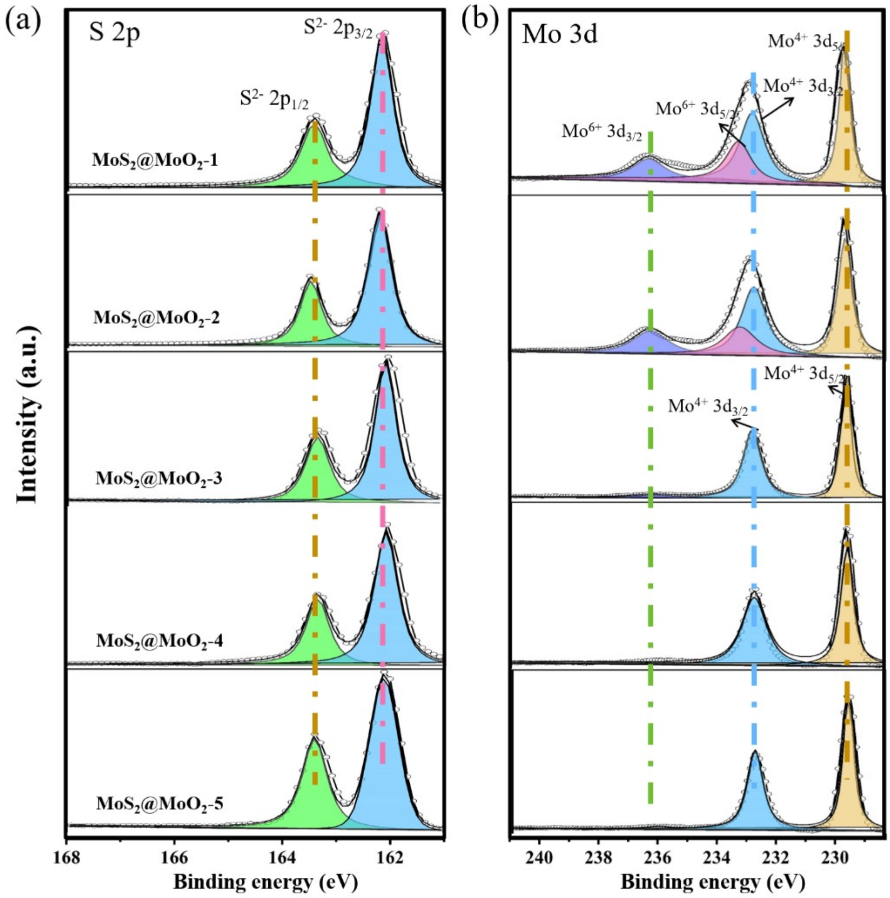

Fig. S7. (a) S 2p, and (b) Mo 3d high-resolution spectra of XPS survey spectrum.

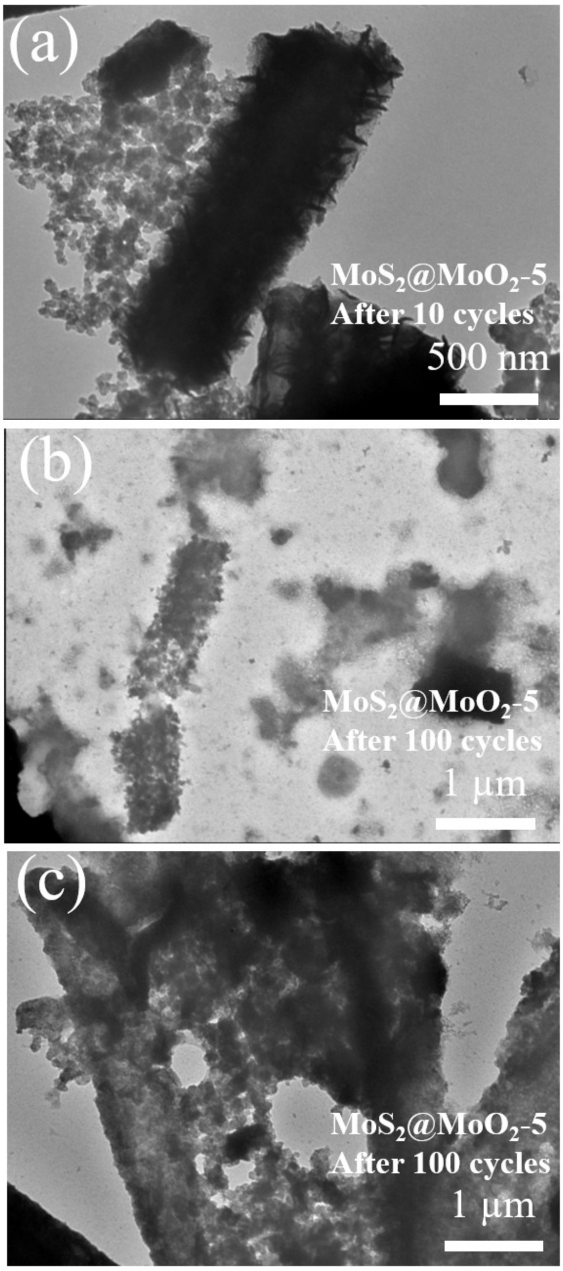

Fig.S8 TEM images of (a) MoS_2@MoO_2-5 electrode after10 cycles, (b-c) after 100 cycles.

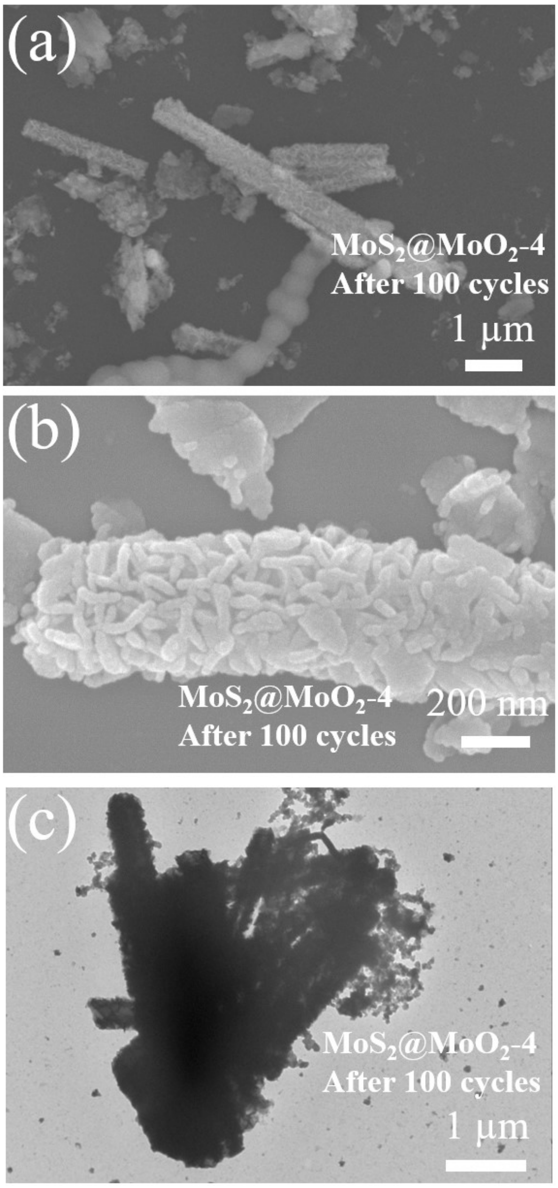

Fig. S9. (a-b) SEM images and (c) TEM images of MoS_2@MoO_2-4 after 100 cycles.

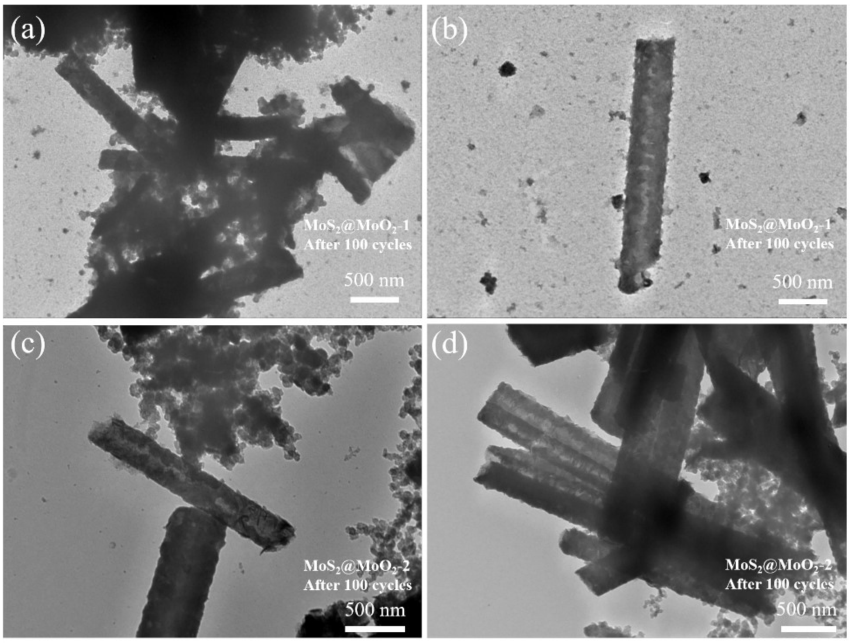

Fig. S10 (a-b) TEM images of MoS_2@MoO_2-1 after 100 cycles; (c-d) TEM images of MoS_2@MoO_2-2 after 100 cycles.

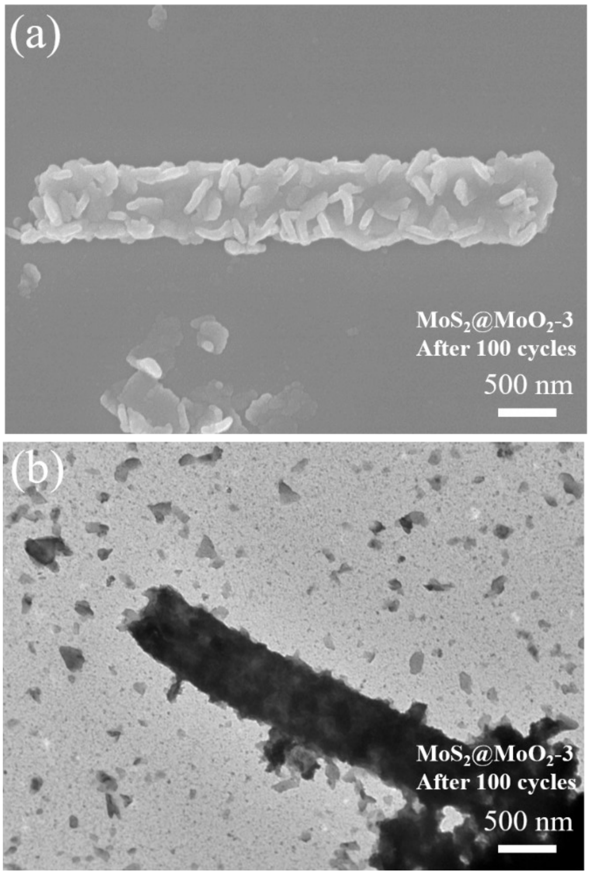

Fig. S11 (a) SEM image and (b) TEM image of MoS_2@MoO_2-3 after 100 cycles.

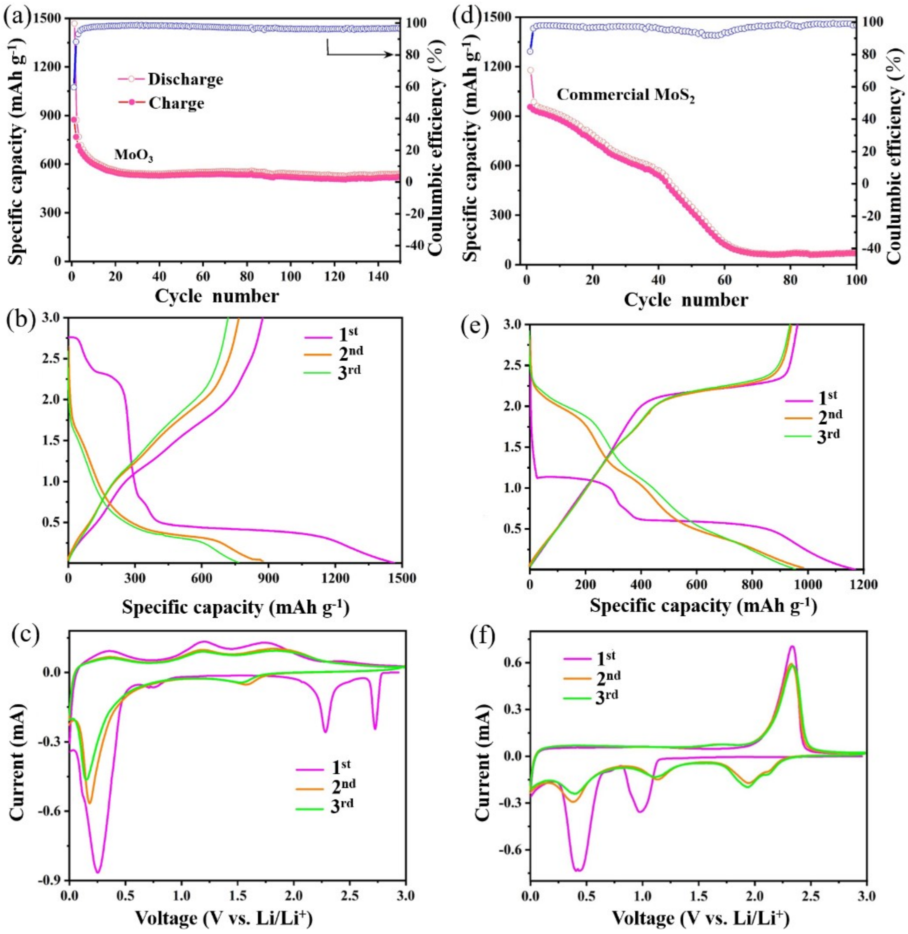

Fig. S12. (a) Cycling performances of MoO_3; (b) Charge-discharge voltage profiles of MoO_3 anodes at a current density of 0.1 C; (c) CV curves of MoO_3 anodes at a scan rate of 0.1 mV s^{-1}; (d) Cycling performances of commercial MoS_2; (e) Discharge-charge voltage profiles of MoS_2 anodes at a current density of 0.1 C; (f) CV curves of MoS_2 anodes at a scan rate of 0.1 mV s^{-1}.

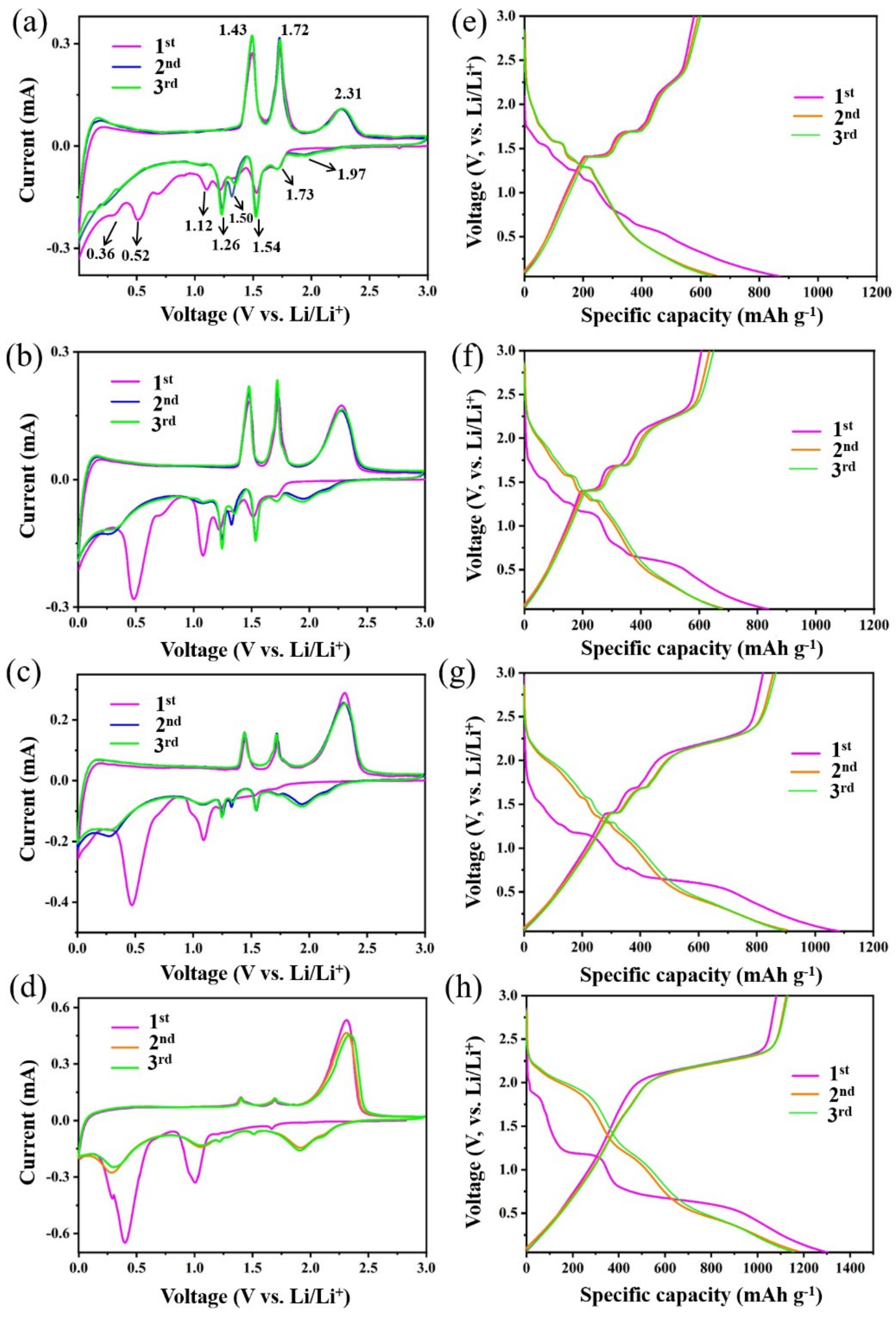

Fig. S13. (a) CV curves of MoS_2@MoO_2-1 anodes at a scan rate of 0.1 mV s^{-1}; (b) CV curves of MoS_2@MoO_2-2 anodes at a scan rate of 0.1 mV s^{-1}; (c) CV curves of MoS_2@MoO_2-3 anodes at a scan rate of 0.1 mV s^{-1}; (d) CV curves of MoS_2@MoO_2-5 anodes at a scan rate of 0.1 mV s^{-1}; (e) Discharge-charge voltage profiles of MoS_2@MoO_2-1 anodes at a current density of 0.1 C; (f) Discharge-charge voltage profiles of MoS_2@MoO_2-2 anodes at a current density of 0.1 C; (g) Discharge-charge voltage profiles of MoS_2@MoO_2-3 anodes at a current density of 0.1 C; (h) Discharge-charge voltage profiles of MoS_2@MoO_2-5 anodes at a current density of 0.1 C.

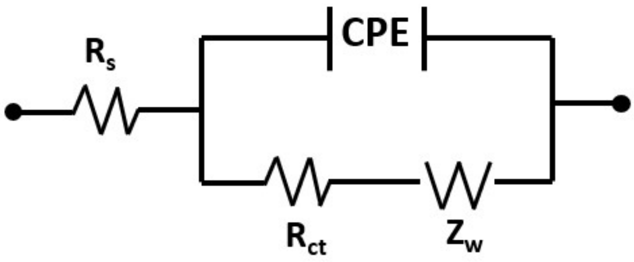

Fig. S14 Equivalent circuit diagrams.

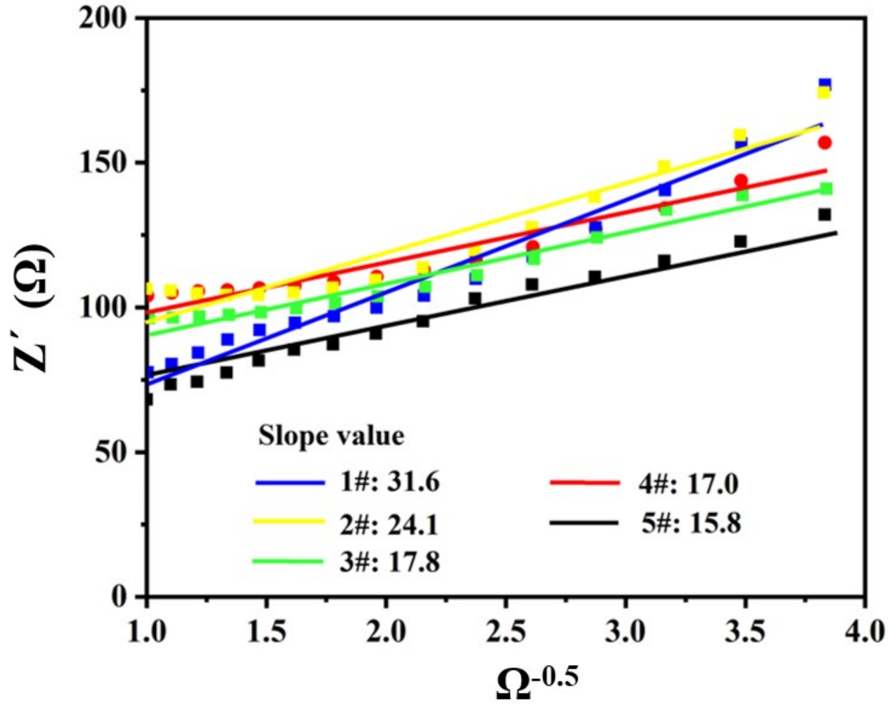

Fig. S15 Z′ as a function of the $\omega^{-0.5}$ plot in the low frequency range (the slope of fitting curves is the Warburg factor, σ_{ω}).

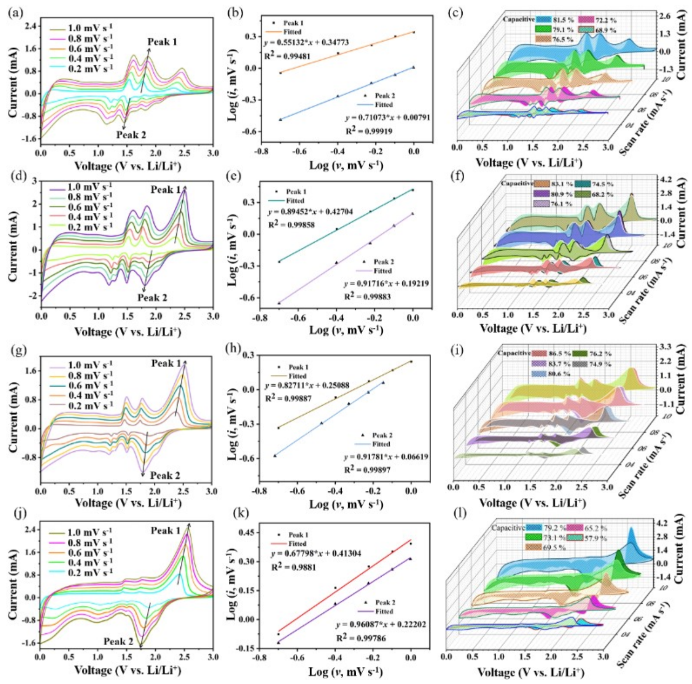

Fig. S16. (a) CV curves of the MoS_2@MoO_2-1 electrode at different scan rate ranging from 0.2 to 1.0 mV s^{-1}; (b) The relationship of the sweep rate and peak current to derive the capacitive properties of MoS_2@MoO_2-1 electrode; (c) Contribution ratio of capacitive and diffusion controlled behaviors at scan various rates for MoS_2@MoO_2-1 electrode; (d) CV curves of of the MoS_2@MoO_2-2 electrode at different scan rate ranging from 0.2 to 1.0 mV s^{-1}; (e) The relationship of the sweep rate and peak current to derive the capacitive properties of MoS_2@MoO_2-1 electrode. (f) Contribution ratio of capacitive and diffusion-controlled behaviors at scan various rates for MoS_2@MoO_2-2 electrode; (g) CV curves of of the MoS_2@MoO_2-3 electrode at different scan rate ranging from 0.2 to 1.0 mV s^{-1}; (h) The relationship of the sweep rate and peak current to derive the capacitive properties of MoS_2@MoO_2-1 electrode. (i) Contribution ratio of capacitive and diffusion-controlled behaviors at scan various rates for MoS_2@MoO_2-3 electrode; (j) CV curves of of the MoS_2@MoO_2-5 electrode at different scan rate ranging from 0.2 to 1.0 mV s^{-1}; (k) The relationship of the sweep rate and peak current to derive the capacitive properties of MoS_2@MoO_2-1 electrode; (l) Contribution ratio of capacitive and diffusion-controlled behaviors at scan various rates for MoS_2@MoO_2-5 electrode.

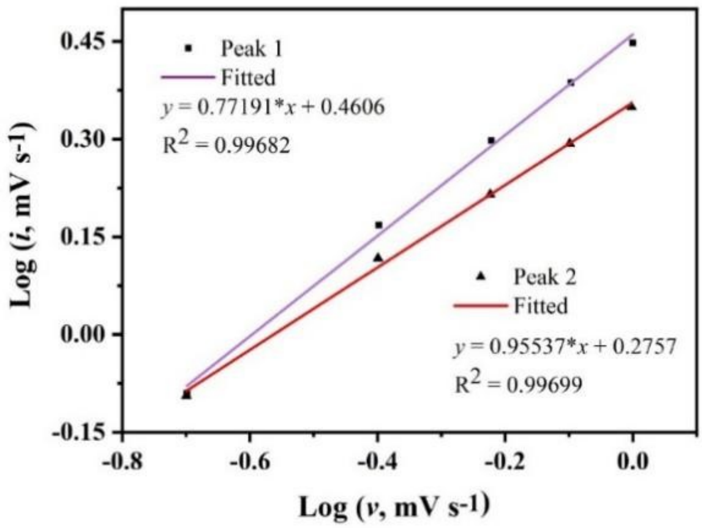

Fig. S17. The relationship of the sweep rate and peak current to derive the capacitive properties of MoS_2@MoO_2-4 electrode.

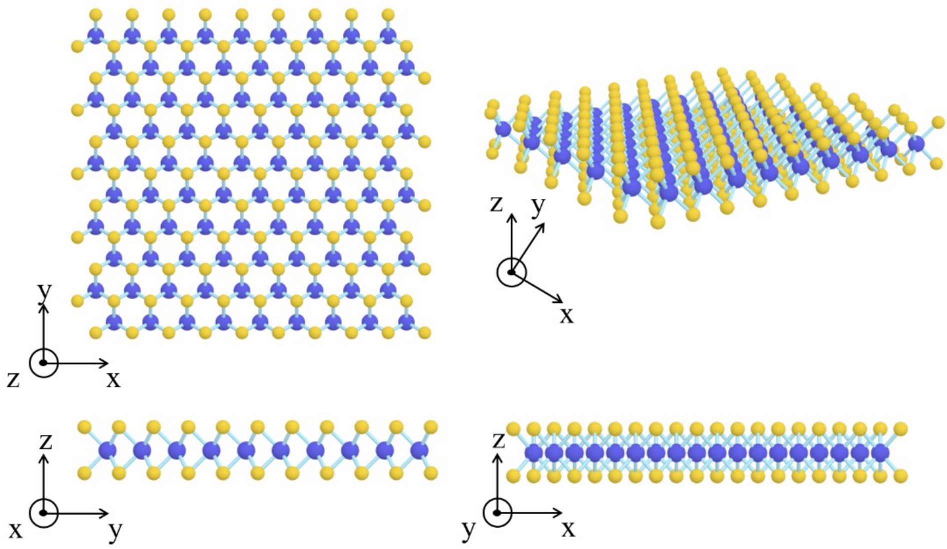

Fig. S18. Molecular models of MoS_2.

Table S1. Layer spacing of the series samples of MoS_2. According to the equations: $2d\sin\theta = n*\lambda$, where n=1, λ=0.15406 nm, and 2θ is value of {002}.

Samples	2θ (°)	Sin θ	d (nm)
MoS_2@MoO_3-1	13.07	0.11381	0.676
MoS_2@MoO_3-2	13.30	0.11583	0.664
MoS_2@MoO_3-3	13.85	0.12062	0.638
MoS_2@MoO_3-4	14.17	0.12334	0.624
MoS_2@MoO_3-5	14.30	0.12446	0.618

Table S2. Layer spacing of the series samples of MoO_2. According to the equations: $2d\sin\theta = n*\lambda$, where n=1, λ=0.15406 nm, and 2θ is value of {011}.

Samples	2θ (°)	Sin θ	d (nm)
MoS_2@MoO_3-1	24.80	0.21940	0.351
MoS_2@MoO_3-2	25.15	0.21771	0.353
MoS_2@MoO_3-3	25.92	0.22427	0.345
MoS_2@MoO_3-4	25.94	0.22444	0.343
MoS_2@MoO_3-5	26.03	0.22520	0.342

Table S3. Summaries of the surface areas, the pore volumes and the average pore diameters of MoO_3, MoS_2@MoO_2-1, MoS_2@MoO_2-2, MoS_2@MoO_2-3, MoS_2@MoO_2-4 and MoS_2@MoO_2-5, respectively.

Samples	Surface Area ($m^2\ g^{-1}$)	Pore Volume ($cm^3\ g^{-1}$)	Average pore Diameter (nm)
MoO_3	10.3	0.031	20.67
MoS_2@MoO_2-1	14.2	0.068	27.23
MoS_2@MoO_2-2	15.0	0.069	16.04
MoS_2@MoO_2-3	17.3	0.040	14.28
MoS_2@MoO_2-4	20.5	0.042	14.13
MoS_2@MoO_2-5	19.2	0.040	14.54

Table S4. The Li^+ diffusion coefficients of five electrode after 100 cycles.

Sample	$\sigma_\omega (\Omega\ s^{-0.5})$	D_{K+} ($cm^2\ s^{-1}$)
MoS_2@MoO_3-1	31.6	$5.71\cdot10^{-13}$
MoS_2@MoO_3-2	24.1	$9.82\cdot10^{-13}$
MoS_2@MoO_3-3	17.8	$1.80\cdot10^{-12}$
MoS_2@MoO_3-4	17.0	$1.98\cdot10^{-12}$
MoS_2@MoO_3-5	15.8	$2.30\cdot10^{-12}$